ANALYSIS OF DYNAMIC CHARACTERISTICS OF FLUID FORCE INDUCED BY LABYRINTH SEAL

Takuzo Iwatsubo, Ryoji Kawai,
Naoya Kagawa, Tetsuya Kakiuchi, and Kazuki Takahara
Kobe University, Rokkodai Kobe
Japan

In this paper flow patterns of the labyrinth seal are experimentally investigated for making a mathematical model of labyrinth seal and to obtain the flow induced force of the seal.

First, the flow patterns in the labyrinth chamber are studied on the circumferential flow using bubble and on the cross section of the seal chamber using aluminum powder as tracers. And next, the fluid force and its phase angle are obtained from the measured pressure distribution in the chamber and the fluid force coefficients are derived from the fluid force and the phase angle. Those are similar to the expression of oil film coefficients.

As the results it is found that the vortexes exist in the labyrinth chambers and its center moves up and down periodically. The pressure drop is biggest in the first stage of chambers and next in the last stage of chambers.

INTRODUCTION

Labyrinth seal are used as the non-contact type seals between rotor and stator of fluid machineries, such as, steam turbines, gas turbines, compressors and so on. To improve the efficiency of these fluid machineries, pressure of the working fluid and rotating speed of rotor tend to become high while the clearance of labyrinth seal is designed narrow to prevent for the leakage flow. As a risk of seeking such a high performance machinery, unstable vibrations of rotor occur and they draw an industrial important problem. The labyrinth seal is considered as one of these vibrations. Unstable vibration induced by the labyrinth seal was first pointed out by Alford(ref. 1), and after that it has been studied by many investigators. Among them, Boyman & Suter(ref. 2) made experimental studies and sketched the flow patterns. In this study, they had interested in the static characteristics of the labyrinth seal, but not in the dynamic characteristic, so, they did not concern with the flow induced force of labyrinth seal. On the other hand, Benckert & Wachter(ref. 3) had interested in the dynamic characteristic and they measured the hydraulic spring coefficients by using the static method. That is, rotor was fixed eccentrically toward casing and the hydraulic spring coefficient was measured by static way. The weak point of this study is not to be able to consider the effect of damping and its effect can not be neglected. On the contrary, Wright(ref. 4) investigated the instability condition of rotors induced by the labyrinth seal force for two seal strips model under many test conditions and also measured the destabilizing fluid force which included the damping coefficient. This study is valuable because it considers the hydraulic spring and damping coefficients, however it lacks generality because the rotor has only two seal strips.

The purpose of this paper is to study the flow patterns, which is needed mathematically to model the flow in the labyrinth seal. Namely, the flow pattern of the cross section and the circumference of the labyrinth chamber are observed. Bubble is used as a tracer for the visualization of the circumference and aluminum powder is also used in that of the cross section, and the photographs of them are taken. Moreover, the flow induced force is measured under the condition of both spinning and whirling motions of the rotor and measuring the change of pressure and of the phase angle in the labyrinth chamber. The eight coefficients, which represent the flow induced force of labyrinth seal by the function of velocity and displacement, i.e. they are correspond to the coefficients of the journal bearing, are obtained.

TEST APPARATUS

The test apparatus to observe the flow patterns and to measure the fluid force is shown in figure 1. In this figure the rotor ① is driven by the three-phase motor ⑩ through the variable-speed drive for spinning motion of ⑨ . The rotor is supported at the upper and the lower part by the eccentric bearings ④ . The dimensions and directions of both eccentricities are set to be equal. Therefore, the rotor is whirled by rotation of the eccentric bearing. The eccentric bearings are driven by the three-phase motor ⑫ through the variable-speed drive ⑪ for whirling motion. Since the rotor and the eccentric bearing are driven by different motors, the rotor can be spun in the same direction as whirl direction (forward) and in the opposite direction (backward), and these spin and whirl speeds are continuously changed from 1.6(Hz) to 5.2(Hz).

The schematic piping of the hydraulic circulating system is shown in figure 2. The working fluid is compressed and transported from the tank 1 to the tank 2. The tank 2 acts as an accumulator, and is installed to lower the pulsation of pressure by the pump using the air which is in the upper part of the tank 2. The working fluid is transported from the tank 2 into the test casing through four pipes, and is transported to the measuring part through the rectifier. The test seals have two or six strips and are the straight-through type seals. After that, the working fluid is returned to the tank 1 by natural draining. Two test casings are prepared, i.e. one is made of acrylic resin for the observation of streamline and the other is made of stainless steel for the measurement of the flow induced force.

The rotating speed of the rotor is measured by the pulse of the notched disk which is installed on the upper end of the rotor. The whirl frequency of the rotor is measured by the measurement of the whirl amplitude of the rotor. The change of pressure by the whirl of rotor is measured through the needle of injector, which is fixed in the measuring point of the test casing where the middle point between two confronted strips corresponds, by the semiconductive pressure transducer. The measured signal current is sent to the signal analyser through the D.C. amplifire and is analyzed.

EXPERIMENT I (Observation of flow patterns)

Two kinds of experiment, that is, experiment I-1 and experiment I-2 , are done using the acrylic resin test casing in experiment I. And two kinds of test seal are prepared, i.e. one has two seal strips and the other has six seal strips. The flow pattern of the cross section of the labyrinth chamber is observed in experiment I-1 and the circumferential flow pattern is observed in experiment I-2 . From the limit of stress of the test casing, two kinds of entrance pressure, i.e. 122.5(kPa) and

147.0(kPa), and three kinds of spinning speed 0(Hz), 2(Hz), and 3(Hz), are tested.

Test procedure of experiment I-1 (Cross section)

To observe the cross section of the labyrinth chamber, the stroboscopic light is thrown through the slit whose clearance is 1.5(mm) as shown in figure 3, and the reflected light of the tracer of aluminum powder is photographed.

Test procedure of experiment I-2 (Circumference)

To observe the circumferential flow of the labyrinth chamber, the light of reflector lamp is used and the motion of vortex in the labyrinth chamber is photographed using bubble tracer.

EXPERIMENTAL RESULTS AND CONSIDERATION

Figures 4 and 5 show the flow patterns of one chamber seal, in which the flow in cross section is shown in figure 4 and the circumferential flow is shown in figure 5. The flow which through the first seal forms the vortex row in the labyrinth chamber. The center of vortex row does not stay and moves sinusoidally as shown in figure 5, and the sinusoidal wave moves in the same direction as spin direction at a lower speed than rotating speed of rotor as shown in figure 6(a). This phenomenon is clear from three photographs of figure 4 that the cross sections of labyrinth chamber are taken. It is found from these photographs that the vortex moves up and down against flow as shown in figure 6(b).

Figures 7 and 8 show the flow pattern of 5 chambers seal. The flow in cross section is shown in figure 7 and the circumferential flow is shown in figure 8. As the case of one chamber seal, the flow in each chamber also forms sinusoidal vortex row. The periods of vortex rows in 5 chambers are almost the same, but there is no particular regularity between the phase angles of the vortex rows. Bubble which through the first seal is big. It means that the pressure drop in the first chamber is high. This result corresponds to the measurement results of the pressure drop in each chamber. As the case of one chamber seal, it is found from figure 7 of the cross sectional photograph that there are vortexes.

EXPERIMENT II (Measurement of fluid force)

Two kinds of experiment, that is, experiment II-1 and experiment II-2, are performed using one chamber seal and 5 chambers seal in experiment II. The fluid force F which acts on the rotor, and the phase angle ϕ between whirl and fluid force, are measured in experiment II-1. The spring coefficients and the damping coefficients of the working fluid are measured in experiment II-2.

Experiment II-1 (Fluid force and phase angle)

The rotating speed is set to the whirl speed, and the change of pressure and its phase angle to the whirling motion are measured in each chamber. In case of one chamber seal, three points of figure 9(b), that is, ①, ②, and ③, are used and in

case of 5 chambers seal, seven points of figure 9(c), that is, ① to ⑦ are used. And the position of these measuring points is (III) of figure 9(a). The changes of pressure in each chamber are measured from ② to ⑥ of figure 9(c) in order. In the analysis by the signal analyser, the 10 Hz-low pass filter is used to protect the noise of high frequency. Parameters are set to be entrance pressure, eccentricity, rotating speed, and direction of rotation. Conditions of experiment II-1 are shown in table 1.

Experiment II-2 (Spring and damping coefficients)

The rotor is spun at the fixed eccentricity without whirling motion, and the circumferential pressure distribution is measured. As in the case of experiment II-1, the measuring points are ① to ⑦ in the position of (III) in figure 9. So, the directions of static eccentricity are changed one after another, its procedure is (III)→(IV)→(I)→(II) in figure 9(a), and the pressure of each eccentric state is measured at the measuring points. Consequently, the circumferential pressure distribution of the statically eccentric rotor is measured. The procedure of measurement is that, first, the pressure in each chamber is measured one by one when the rotor's eccentric direction is one of four directions ((I) to (IV) in figure 9(a)) and next the direction of eccentricity is changed and the pressure is measured. Conditions of the experiment II-2 are shown in table 2.

ANALYSIS OF MEASURED DATA

The data obtained in experiment II are the maximum change of pressure ΔP_{max}, the phase angle of pressure to the whirl motion $\angle\phi$ and the change of the circumferential pressure distribution $\Delta P'$ when the rotor is spun without whirl. So, first, the x and the y directional force F_{xo} and F_{yo} are obtained from ΔP_{max} and $\angle\phi$ when the rotor is whirling. Next, the principal spring coefficient K_{xx} and the cross coupled spring coefficient K_{yx} are obtained from $\Delta P'$. And last, the principal damping coefficient C_{yy} and the cross coupled damping coefficient C_{xy} are calculated using the equation of fluid force and the expression is similar to that of the journal bearing.

It is assumed that the circumferential pressure distribution in the whirling motion is circular and the center of it is O_p as shown in figure 10. Thus, the change of the circumferential pressure distribution in the chamber ΔP is given as;

$$\Delta P = \Delta P_{max} \cos(\varphi + \phi - \pi) \tag{1}$$

The x and y direction components F_{xo} and F_{yo} of the fluid force are obtained by using equation (1).

$$F_{xo} = -\int_0^{2\pi} (\Delta P \cos\varphi)\, \ell R_s \, d\varphi$$

$$= -\ell R_s \pi \Delta P_{max} \cos(\pi - \phi) \tag{2}$$

$$F_{yo} = -\int_0^{2\pi} (\Delta P \sin\varphi)\, \ell R_s \, d\varphi$$

$$= -\ell R_s \pi \Delta P_{max} \sin(\pi - \phi) \tag{3}$$

Then the fluid force and its phase angle acting on the rotor are as follows;

$$|F_o| = \sqrt{F_{xo}^2 + F_{yo}^2} \tag{4}$$

$$\phi = \cos^{-1} \frac{F_{xo}}{F_o} \tag{5}$$

where R_s is radius of rotor and ℓ is strip pitch.

On the other hand, K_{xx} and K_{yx} are obtained from the change of the circumferential pressure distribution $\Delta P'$ when the rotor is spun and no whirl with the fixed eccentricity,

$$K_{xx} = \frac{1}{e} \int_0^{2\pi} (\Delta P' \cos\varphi)\, \ell R_s d\varphi \tag{6}$$

$$K_{yx} = \frac{1}{e} \int_0^{2\pi} (\Delta P' \sin\varphi)\, \ell R_s d\varphi \tag{7}$$

where e is eccentricity of rotor. $\Delta P'$ are measured for four cases, that is, $\varphi=0$, $\varphi=\pi/2$, $\varphi=\pi$, and $\varphi=3\pi/2$, and are approximated to a circular distribution, as the case of ΔP, as follows;

$$\Delta P' = \Delta P'_{max} \cos(\varphi + \phi' - \pi) \tag{8}$$

where $\Delta P'_{max}$ is the maximum change of pressure and ϕ' is the phase angle between the position of $\Delta P'_{max}$ and the maximum clearance.

So, the principal spring coefficient K_{xx} and the cross coupled spring coefficient K_{yx} are obtained as follows;

$$K_{xx} = \frac{1}{e} \ell R_s \pi \Delta P'_{max} \cos(\pi - \phi) \tag{9}$$

$$K_{yx} = \frac{1}{e} \ell R_s \pi \Delta P'_{max} \sin(\pi - \phi) \tag{10}$$

Last, the expressions of fluid force induced by labyrinth seal are obtained as follows;

$$F_x = -(K_{xx} + \omega_n C_{xy})x - (K_{xy} - \omega_n C_{xx})y \tag{11}$$

$$F_y = -(K_{yx} + \omega_n C_{yy})x - (K_{yy} - \omega_n C_{yx})y \tag{12}$$

where F_x and F_y are the function of time and ω_n is critical speed of rotor system. Then equations (11) and (12) are considered at the same time as equations (2) to (5) as follows;

$$F_{xo} = -K_{xx} e - \omega_n C_{xy} e \tag{13}$$

$$F_{yo} = -K_{yx} e - \omega_n C_{yy} e \tag{14}$$

Substituting equations (2), (3), (9) and (10) into equations (13) and (14), the cross coupled damping coefficient C_{xy} and the principal damping coefficient C_{yy} are obtained.

EXPERIMENTAL RESULTS AND DISCUSSION

Experiment II-1 (Fluid force and phase angle)

Figure 11 shows an example of wave mode of the signal analyser. The upper part is the wave of the rotor's whirl, and the lower part is that of the pressure change in the chamber. The noise of this wave is pressure disturbance induced by turbulent flow. It is found from figure 11 that there is phase lag between whirl and fluid force.

Experimental results of one chamber seal are shown in figures 12 and 13. In the case of one chamber seal, the fluid force increases with the increase of eccentricity in every condition of both entrance pressures and whirl directions. In many cases, the fluid force increases with the increase of rotating speed. But in the cases of the high entrance pressure and forward precession the fluid force tends to decrease with more than a certain rotating speed. The phase angle ϕ is constant, of which value is about $3\pi/2$(rad) in all cases.

Experimental results of 5 chambers seal are shown in figures 14 to 19. First, the discussions about the forward precession are as follows. The fluid force in each chamber increases with the increase of the entrance pressure. The fluid force in the 1st chamber is more remarkably affected than the others by the rotating speed. The fluid force in the other chambers varies hardly or increases slightly with the increase of the rotating speed. And the fluid force increases with the increase of the eccentricity. The change of fluid force is shown in figure 16. This is the case that the rotating speed is 3.1(Hz) and the tendencies of the fluid force do not change in the other cases. The fluid force in the 2nd chamber decreases, and in the other chambers after the 3rd chamber it gradually increases. The fluid force of the whole labyrinth seal F increases with the increase of rotating speed, entrance pressure or eccentricity (fig. 15). The phase angle ϕ is constant at about $3\pi/2$(rad) and has no relations to entrance pressure, rotating speed, and eccentricity, except for the case in the 2nd chamber. The phase angle in the 2nd chamber is changed by conditions. The reason of this phenomenon is considered as follows. Since the fluid force in the 2nd chamber is small, there is no remarkable difference between the pressure disturbance induced by turbulent flow and the change of pressure induced by whirl. Then, to obtain the accurate phase angle is difficult. In the case that eccentricity is large i.e. 1.0(mm) and the fluid force is greater than the other cases, the phase angle ϕ is constant by about $3\pi/2$(rad). Thus, it is considered that the phase angles ϕ in all chambers are constant by about $3\pi/2$(rad) and have no relation to parameters. In case of backward precession, the tendency of the fluid force is almost same as the case of forward precession. And the fluid force of backward precession is more remarkably affected than that of forward precession by the rotating speed.

Experiment II-2 (Spring and damping coefficients)

Part of experimental results of the spring and damping coefficients are shown in figures 20 to 31. Variation in each figure may depend on the accuracy of instrument and measurement. K_{xx} and K_{yx} have no relation to the rotating speed of rotor. K_{xx} increases with the increase of entrance pressure, but K_{yx} has no relation to entrance pressure. K_{xx} and K_{yx} decrease during the working fluid flows from the 1st chamber to the 5th chamber. C_{yy} and C_{xy} have no relation to entrance pressure and rotating speed. And C_{xy} increases during the working fluid flows from the 1st chamber to the 5th chamber.

CONCLUSIONS

In this paper, the flow patterns of one chamber and 5 chambers seals are investigated, and the fluid force and its phase angle, and the coefficients of fluid force are experimentally obtained. The conclusions are as follows:

(1) In the chamber, the vortex forms the sinusoidal wave and its wave moves in the same direction of rotation in the circumferential direction. Observing a certain cross section of seal chamber, the center of vortex moves up and down periodically.

(2) The fluid force and its phase angle of one chamber seal are qualitatively agree with 5 chambers seal.

(3) The fluid force increases with the increase of entrance pressure, rotating speed or eccentricity.

(4) The fluid force in the 1st chamber and the 5th chamber of the 5 chambers seal, that is, the fluid force of entrance and exit part of labyrinth seal, is great, and the fluid force in the middle region of labyrinth seal is small.

(5) The phase angle of fluid force is constant and has no relation to all parameters.

(6) The principal spring coefficient increases with the increase of entrance pressure, and it decreases from the 1st chamber to the 5th chamber. The damping coefficients have no relation between entrance pressure and rotating speed.

This study is supported by Scientific Research Fund of the Ministry of Education No.56550180 (1981-1982) and No.58550172 (1983).

REFERENCES

(1) Alford, J. S.: Protecting Turbomachinery From Self-Excited Rotor Whirl. Trans. ASME, J. Engng. Power, Oct. 1965, pp. 333-344.

(2) Boyman, T.; and Suter, P.: Transport Phenomena in Labyrinth-Seals of Turbomachines. Institut de Thermique Appliquée CH-1015 Lausanne, Switzerland, pp. 8.1-8.10.

(3) Benckert, H.; and Wachter, J.: Flow Induced Spring Coefficients of Labyrinth Seals for Application in Rotor Dynamics. NASA Lewis, Conference Publication 2133, Rotordynamic Instability Problems in High-Performance Turbomachinery, 1980, pp. 189-212.

(4) Wright, D. V.: Rotor Dynamic Instability. ASME AMD, Vol. 55, 1983, pp. 19.

TABLE 1. - EXPERIMENT Ⅱ-1
EXPERIMENTAL CONDITION

ENTRANCE PRESSURE (kPa)		122.5 147.0 171.5 196.0
ECCENTRICITY (mm)		0.5 0.75 1.0
ω_n/ω		1.0
ω	FORWARD (Hz)	1.9 - 5.2 STEP 0.3
	BACKWARD (Hz)	1.9 - 4.3 STEP 0.3
NUMBER OF CHAMBER		1 5

TABLE 2. - EXPERIMENT Ⅱ-2
EXPERIMENTAL CONDITION

ENTRANCE PRESSURE (kPa)	122.5 147.0 171.5 196.0
ECCENTRICITY (mm)	1.0
WHIRLING SPEED (Hz)	0.0
ROTATING SPEED (Hz)	1.9 - 5.2 STEP 0.3
NUMBER OF CHAMBER	1 5

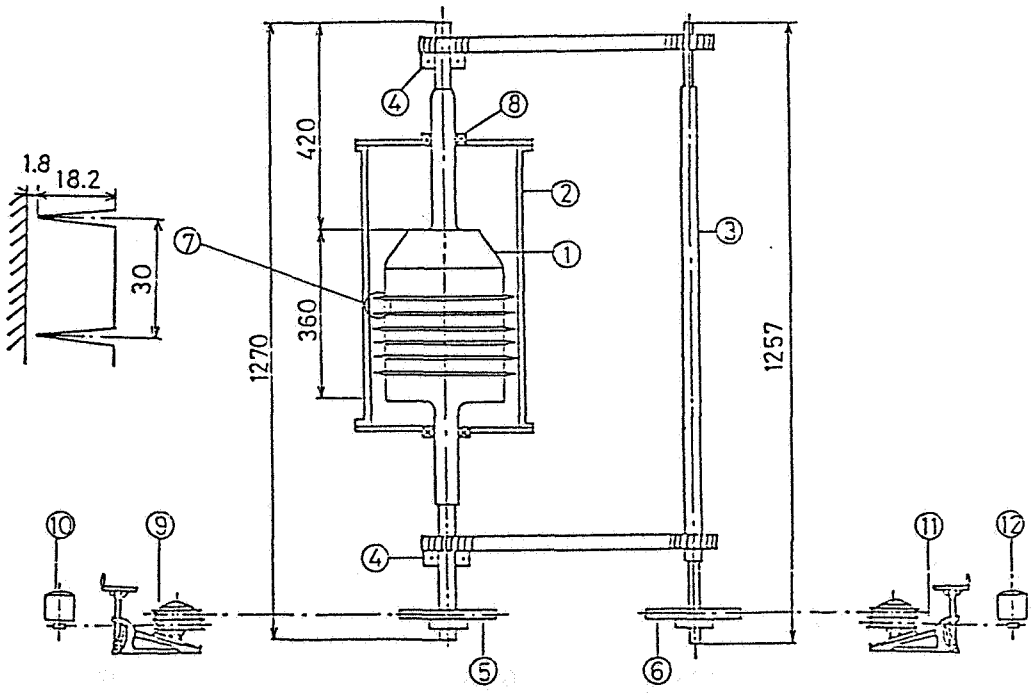

Figure 1. - The schematic layout of the test apparatus.

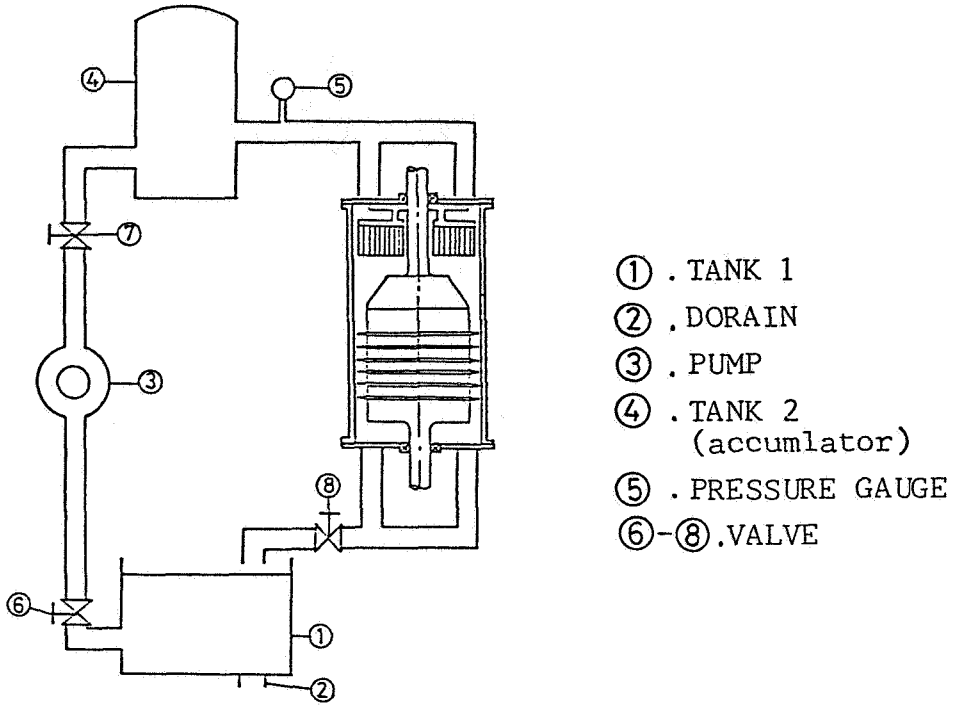

Figure 2. - The schematic piping of the circulating system

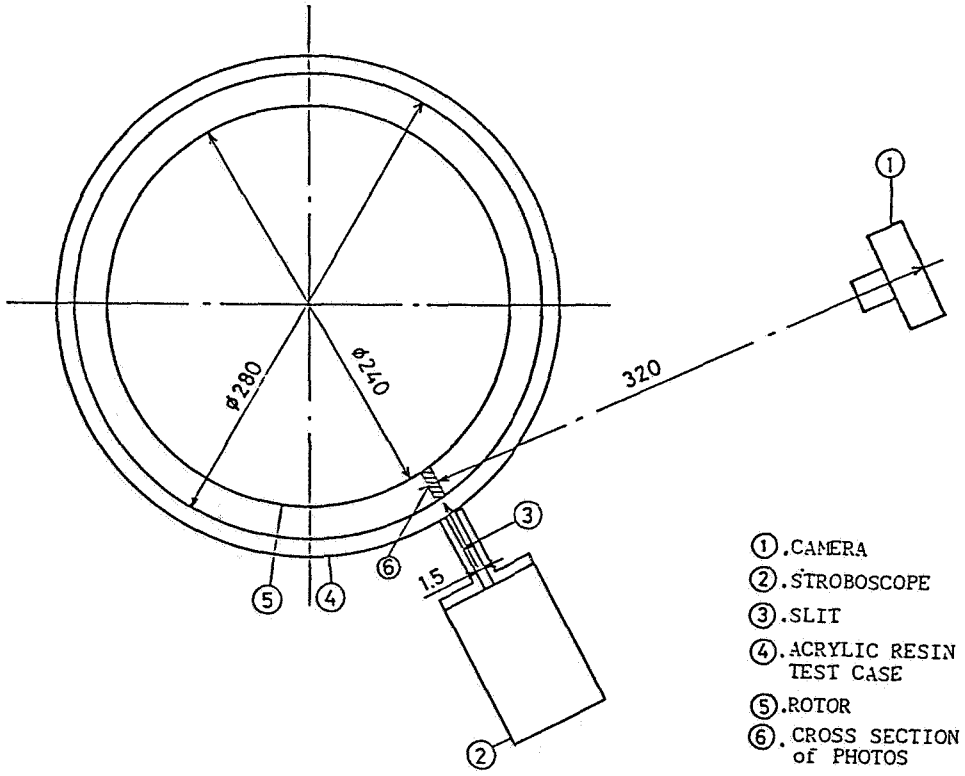

Figure 3. - The schematic layout of the visualizational apparatus.

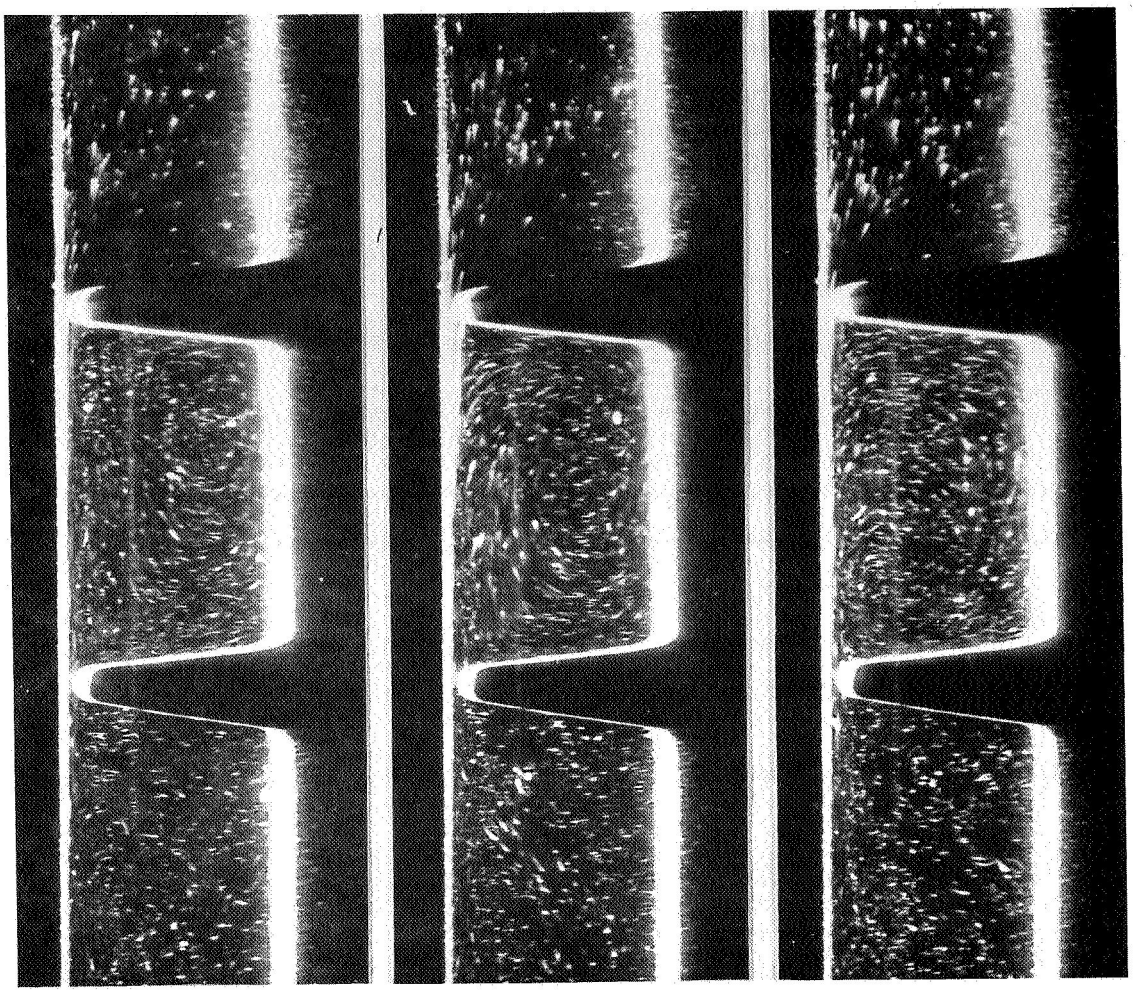

Figure 4. - Cross section of one chamber seal.

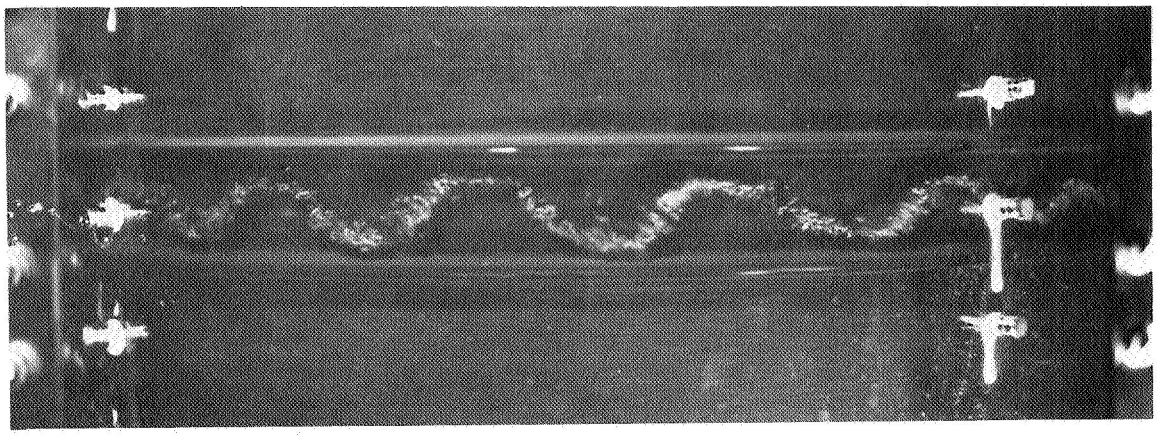

Figure 5. - The movement of vortex row in one chamber seal.

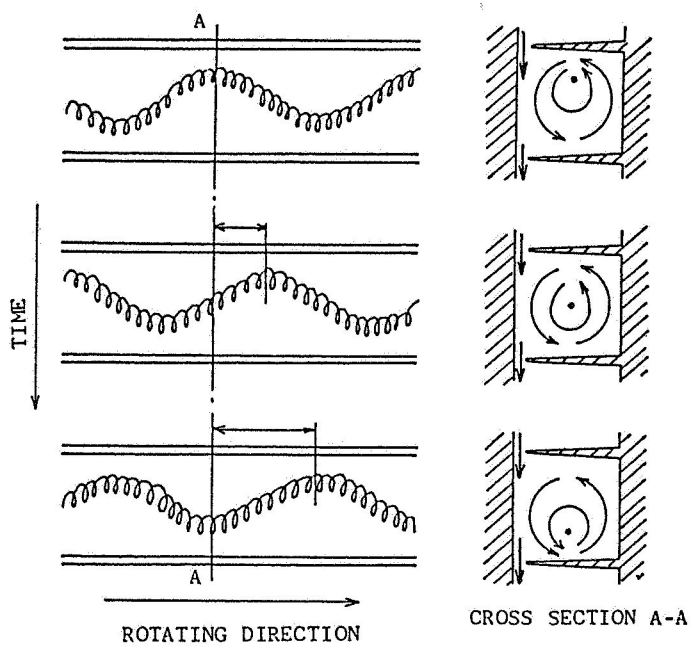

(a) (b)

Figure 6. - The movement of vortex row.

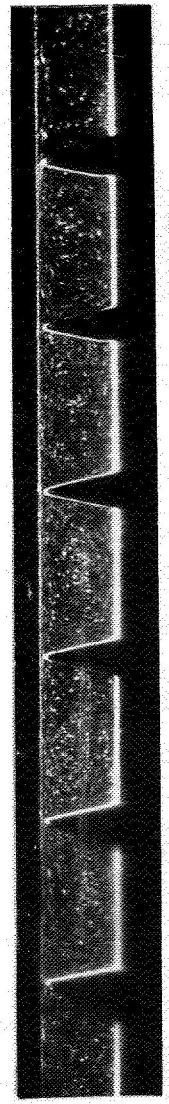

Figure 7. - Cross section of 5 chambers seal.

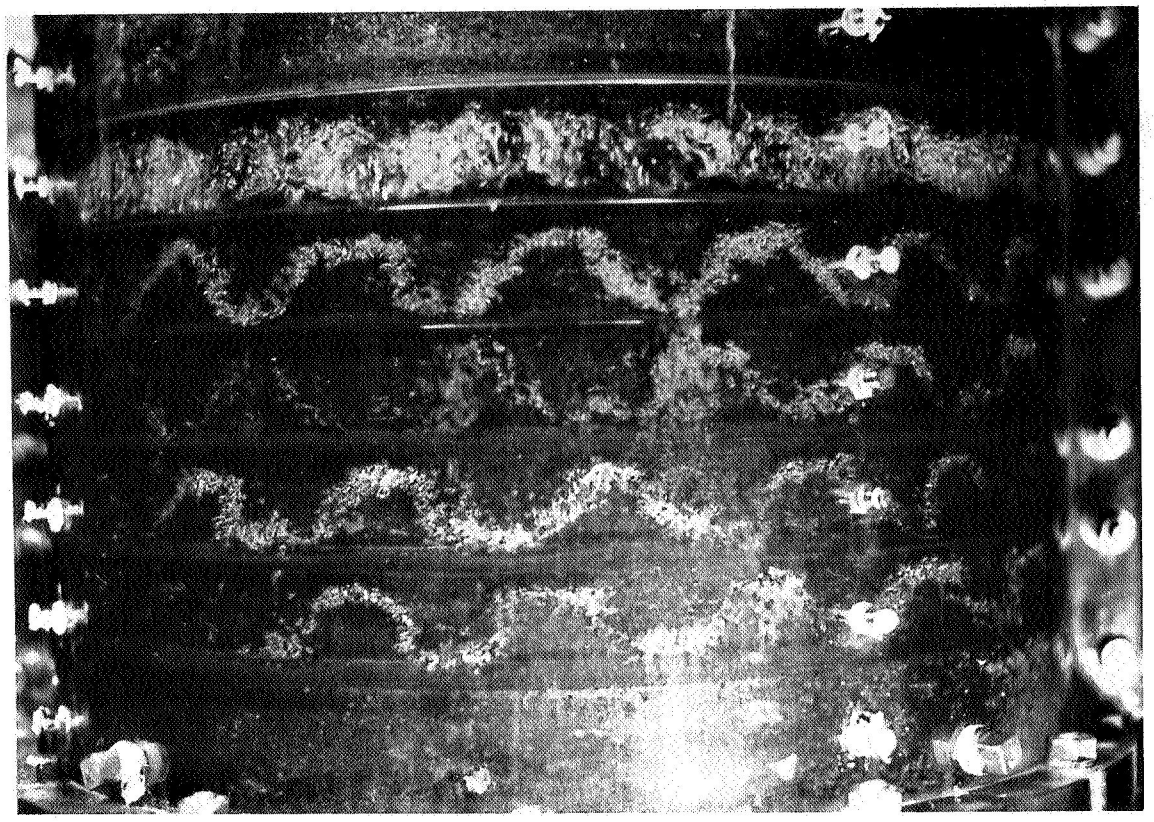

Figure 8. - The movement of vortex row in 5 chambers seal.

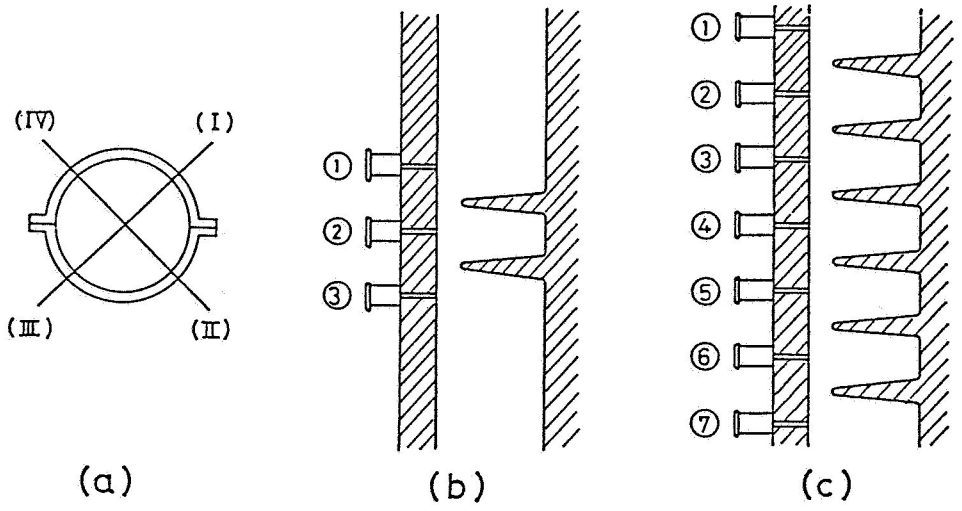

Figure 9. - The measuring points of pressure installed on the test casing.

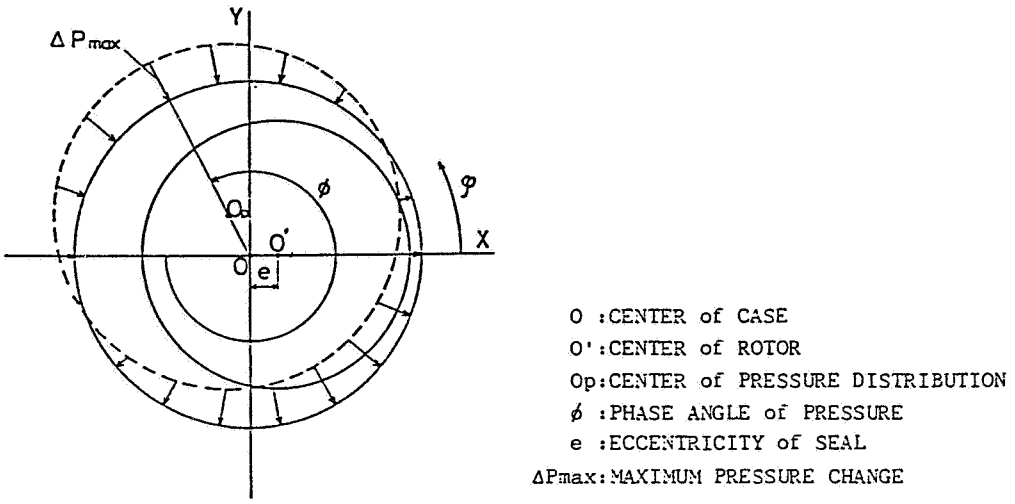

Figure 10. - The assumption of the circumferential pressure distribution.

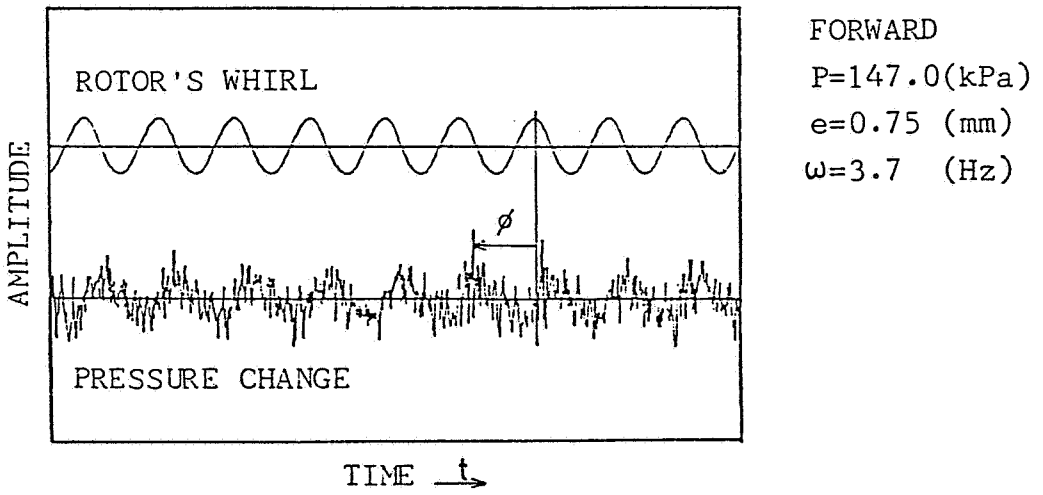

Figure 11. - An example of the analytic wave.

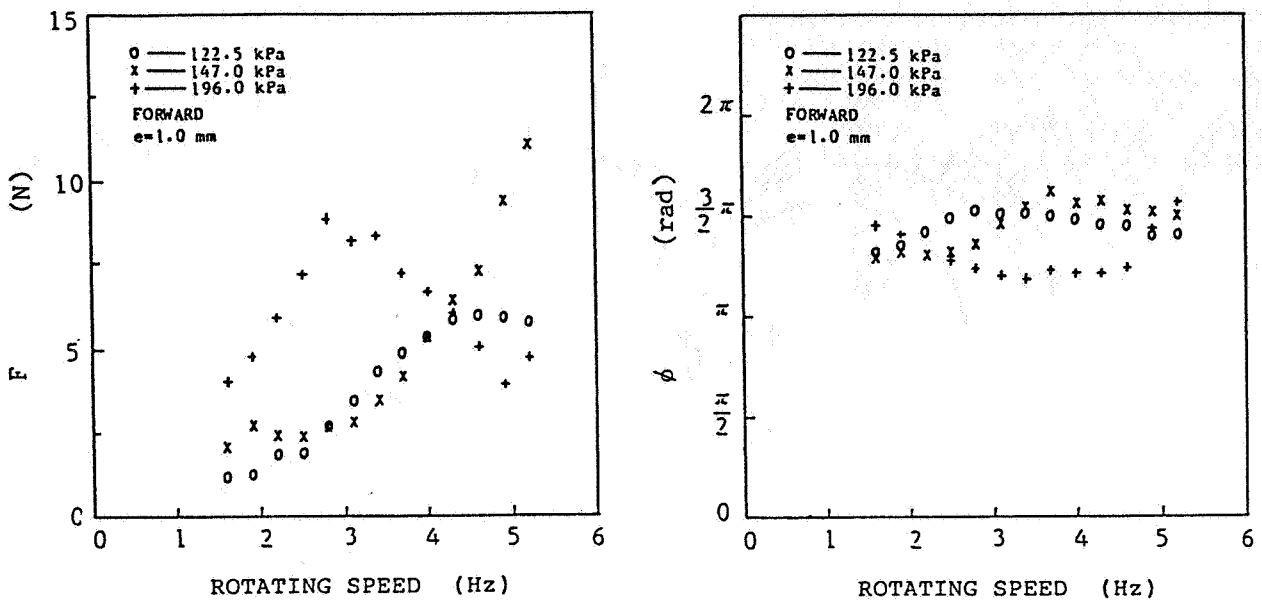

Figure 12. - Fluid force and phase angle of one chamber seal.

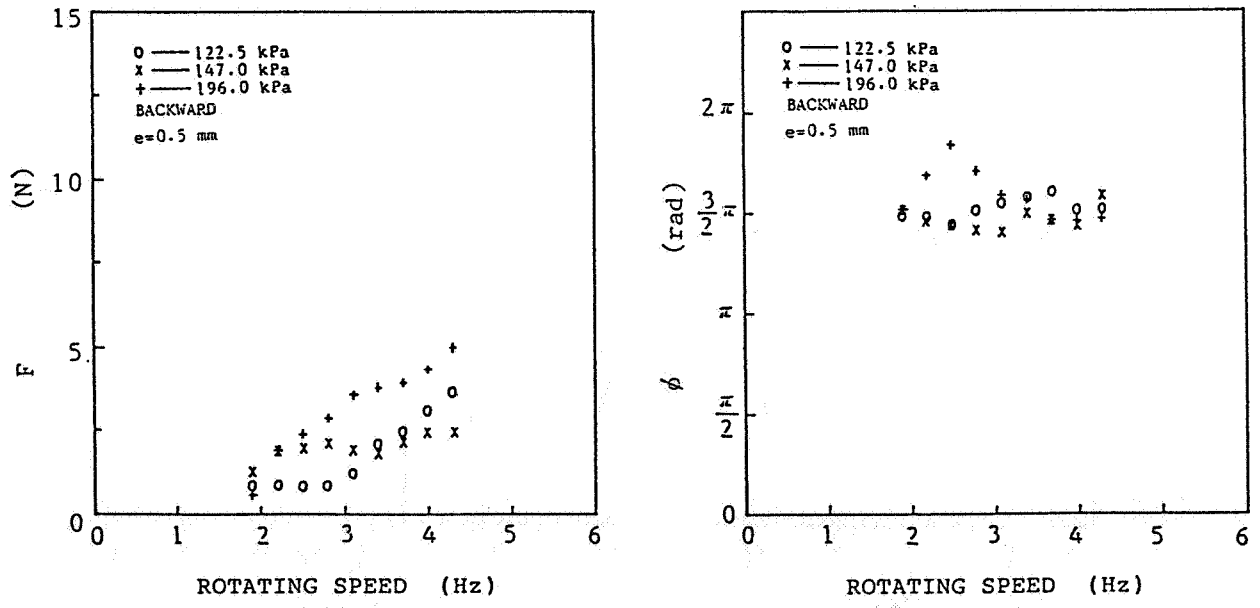

Figure 13.- Fluid force and phase angle of one chamber seal.

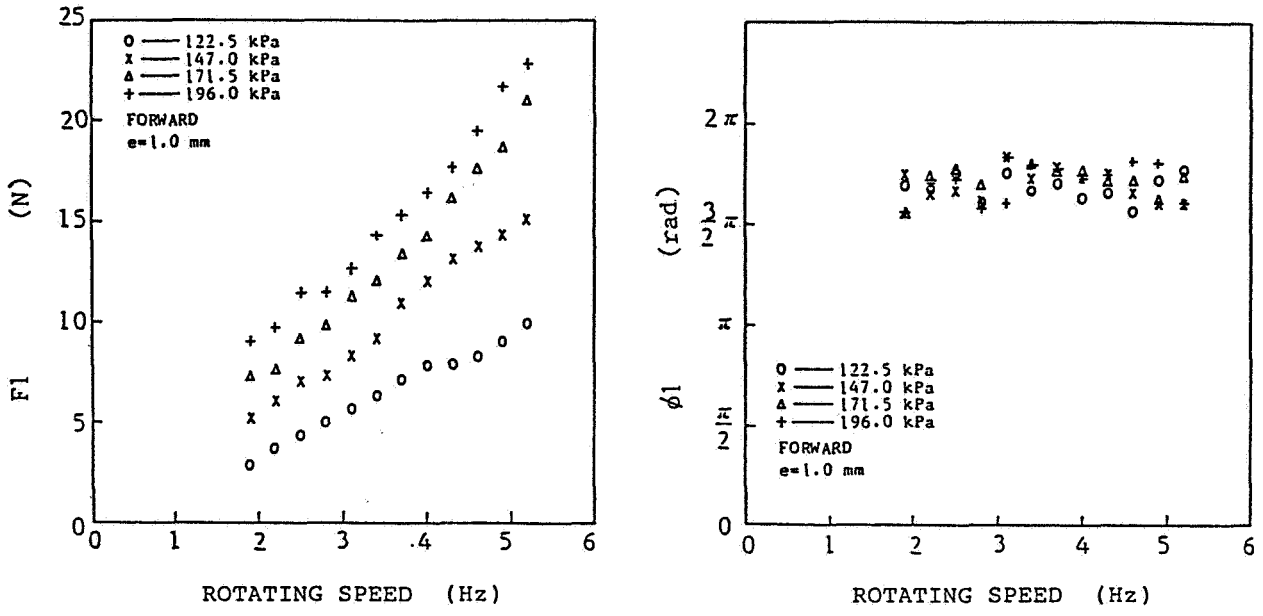

(a)

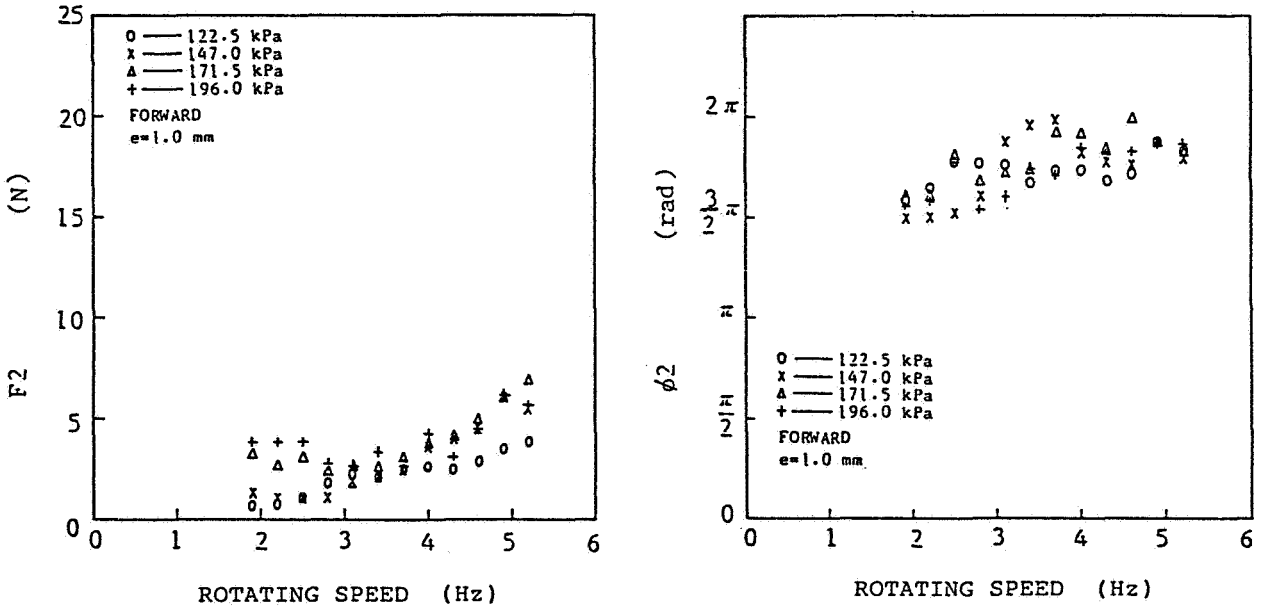

(b)

Figure 14.- Fluid force and phase angle of 5 chambers seal.

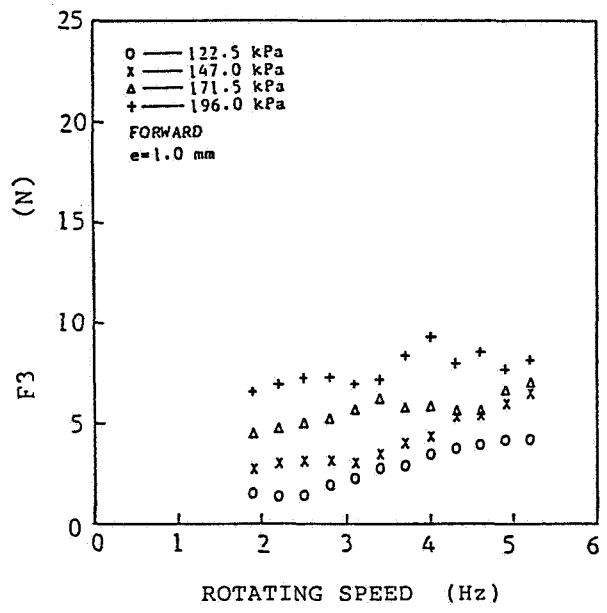
o —— 122.5 kPa
x —— 147.0 kPa
Δ —— 171.5 kPa
+ —— 196.0 kPa
FORWARD
e=1.0 mm
F3
(N)
ROTATING SPEED (Hz)

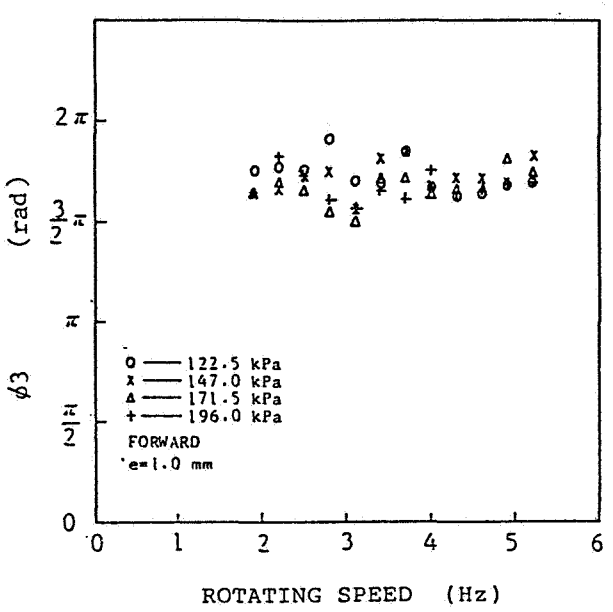
o —— 122.5 kPa
x —— 147.0 kPa
Δ —— 171.5 kPa
+ —— 196.0 kPa
FORWARD
e=1.0 mm
φ3
(rad)
ROTATING SPEED (Hz)

(c)

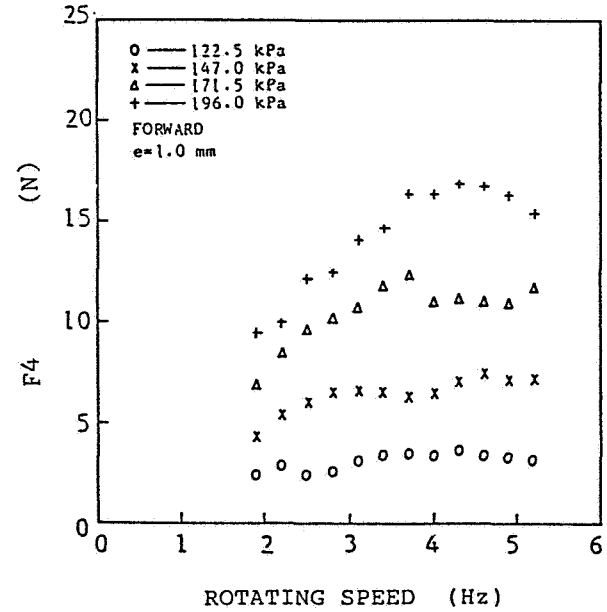
o —— 122.5 kPa
x —— 147.0 kPa
Δ —— 171.5 kPa
+ —— 196.0 kPa
FORWARD
e=1.0 mm
F4
(N)
ROTATING SPEED (Hz)

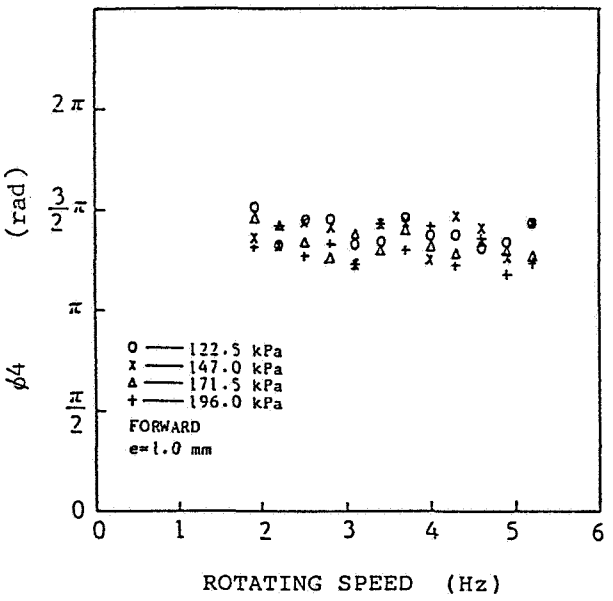
o —— 122.5 kPa
x —— 147.0 kPa
Δ —— 171.5 kPa
+ —— 196.0 kPa
FORWARD
e=1.0 mm
φ4
(rad)
ROTATING SPEED (Hz)

(d)

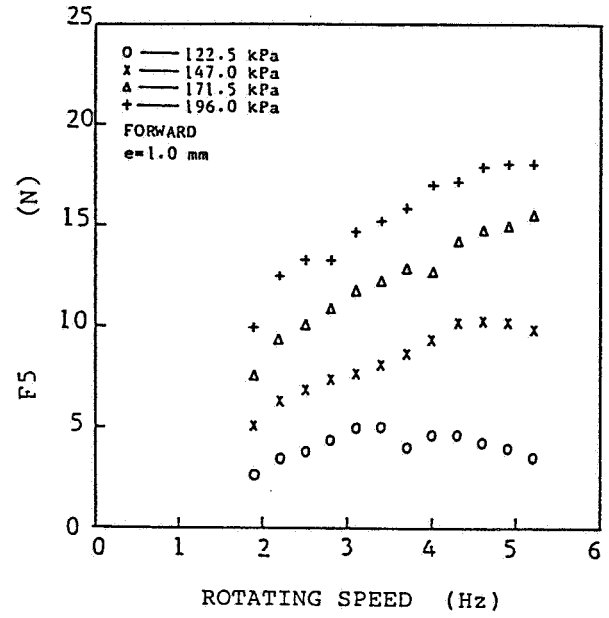

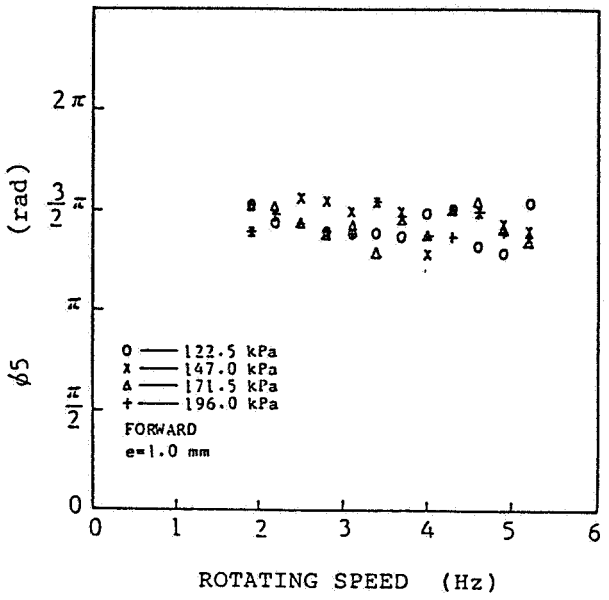

(e)

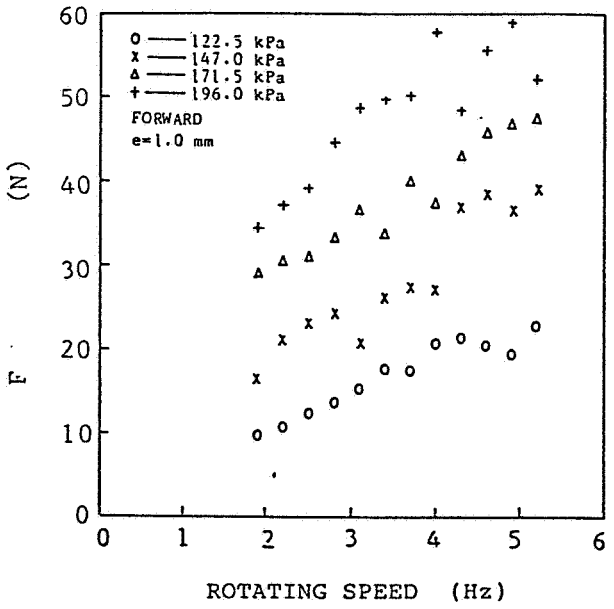

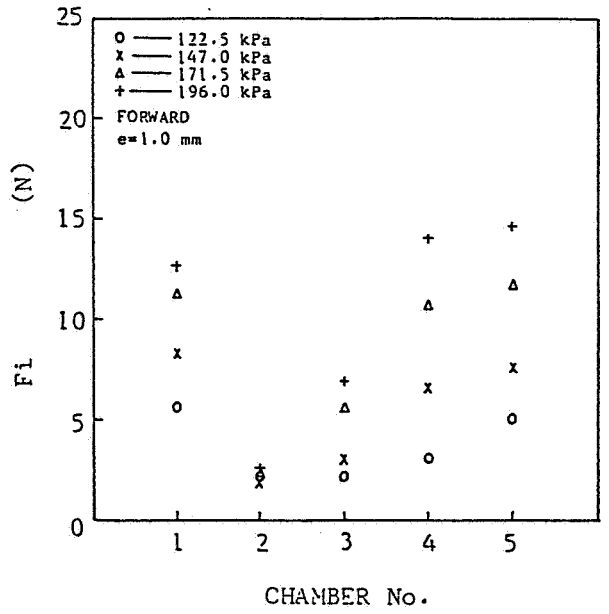

Figure 15. - Fluid force of the whole labyrinth seal.

Figure 16. - Fluid force in each chamber.

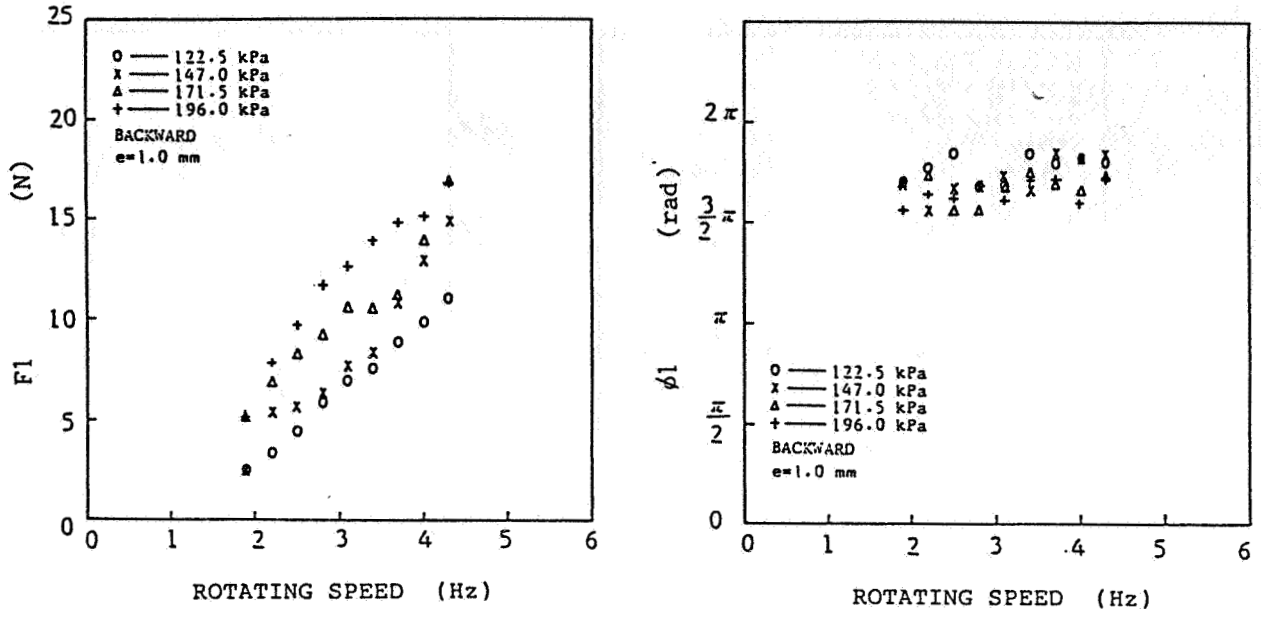

Figure 17. - Fluid force and phase angle of 5 chambers seal.

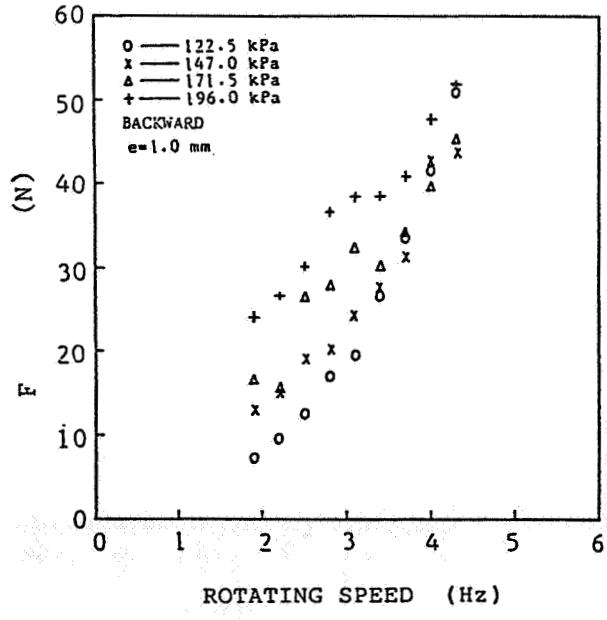

Figure 18. - Fluid force of the whole labyrinth seal.

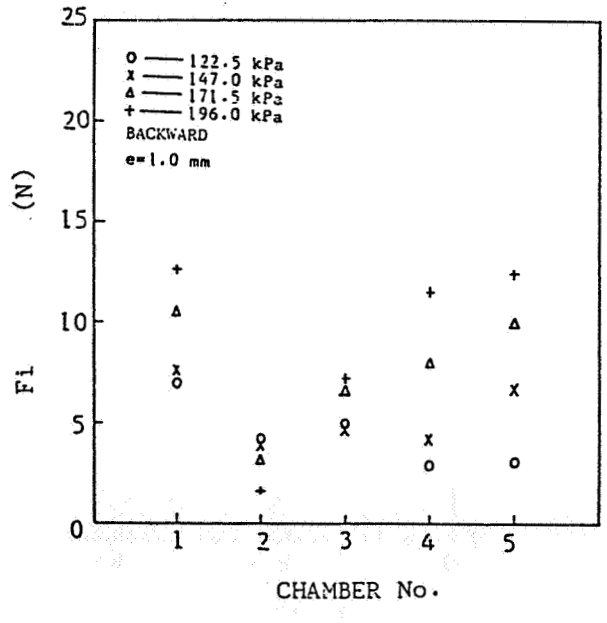

Figure 19. - Fluid force in each chamber.

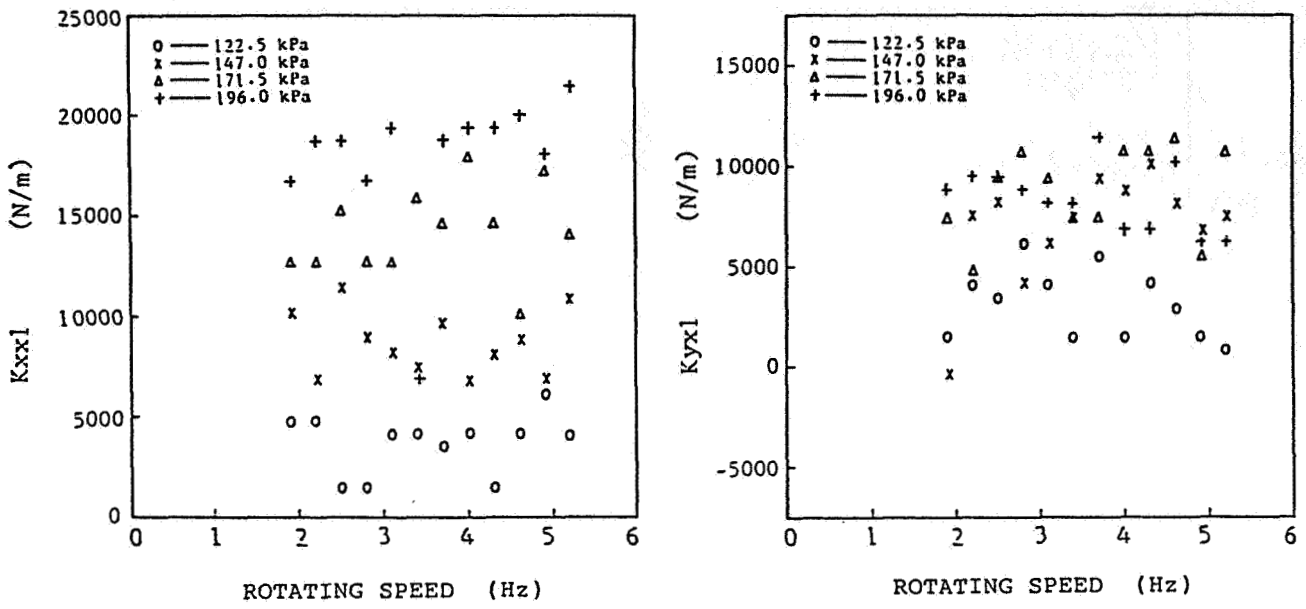

Figure 20. - Spring coefficients in the 1st chamber

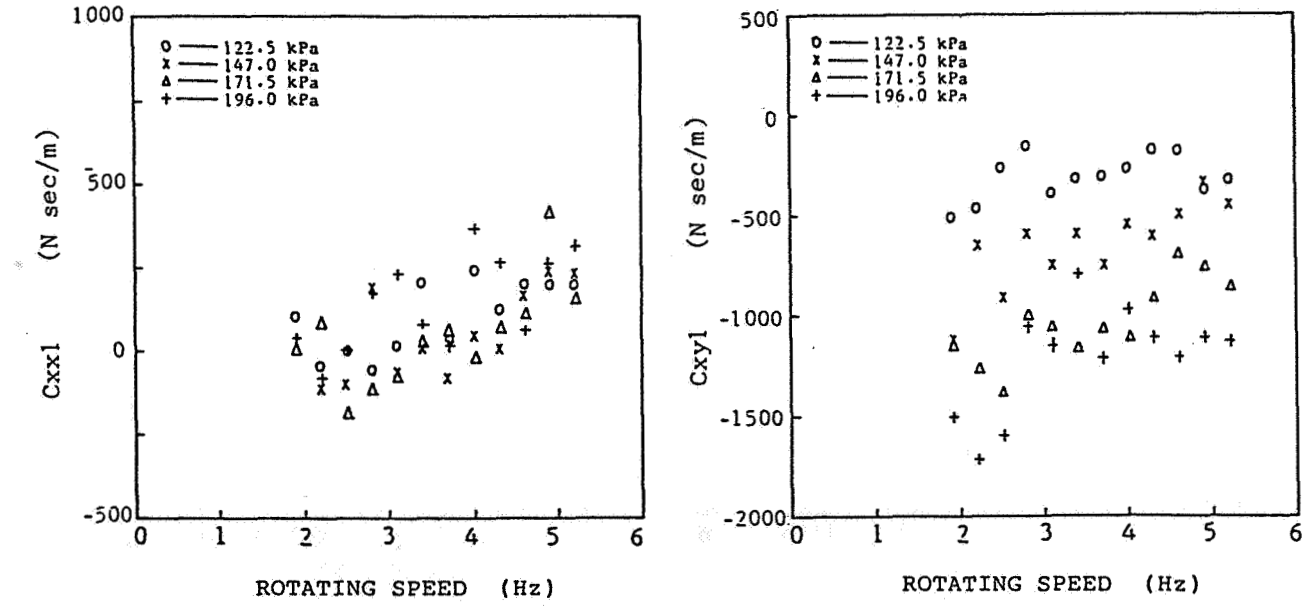

Figure 21. - Damping coefficients in the 1st chamber

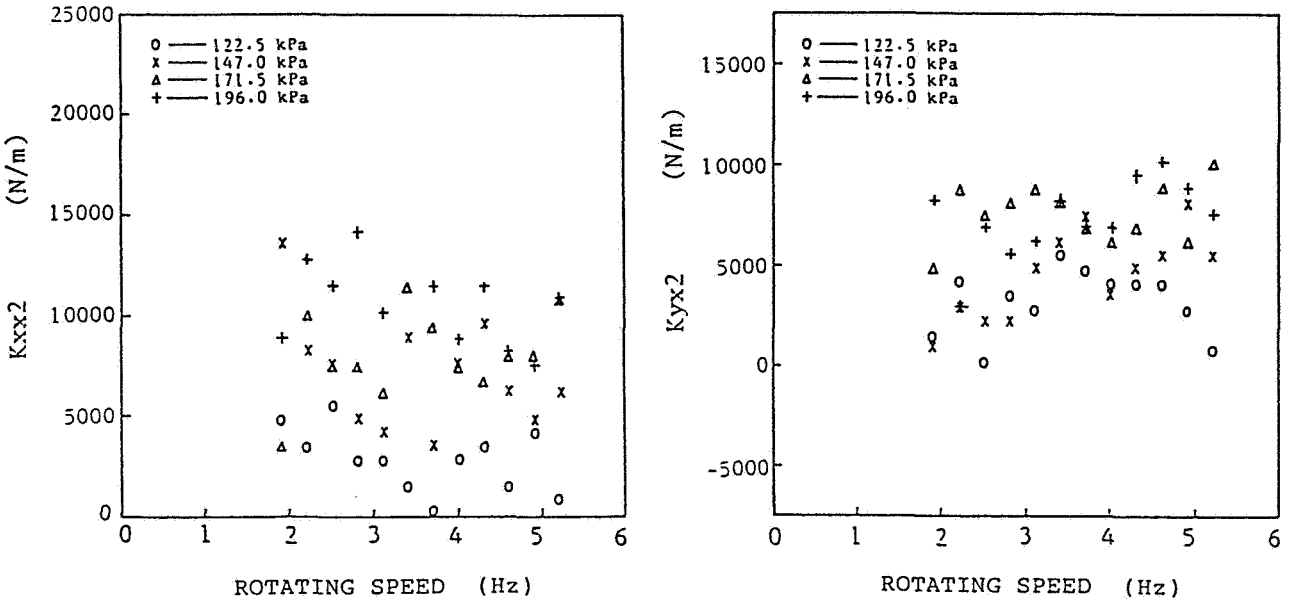

Figure 22. - Spring coefficients in the 2nd chamber

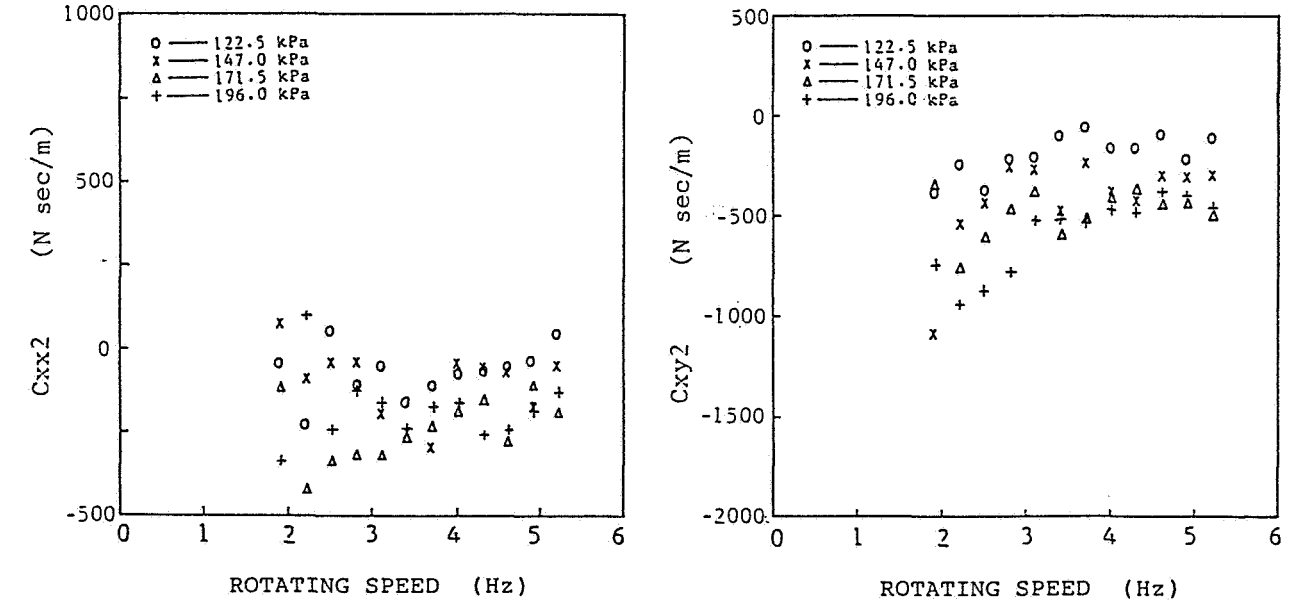

Figure 23. - Damping coefficients in the 2nd chamber

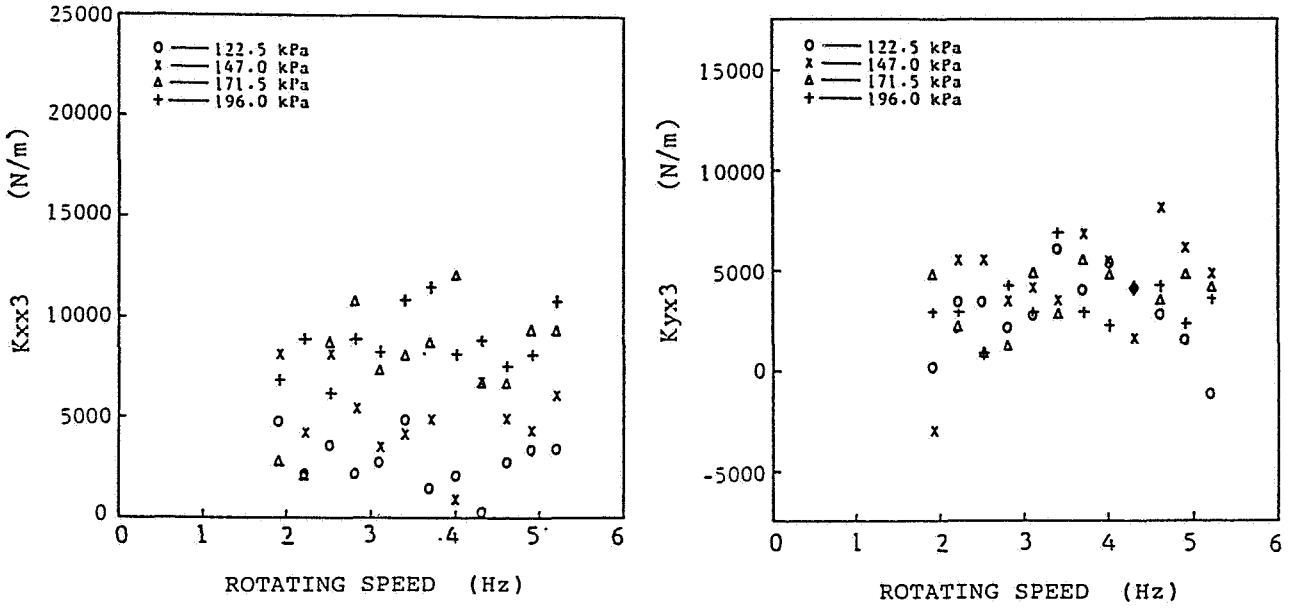

Figure 24. - Spring coefficients in the 3rd chamber

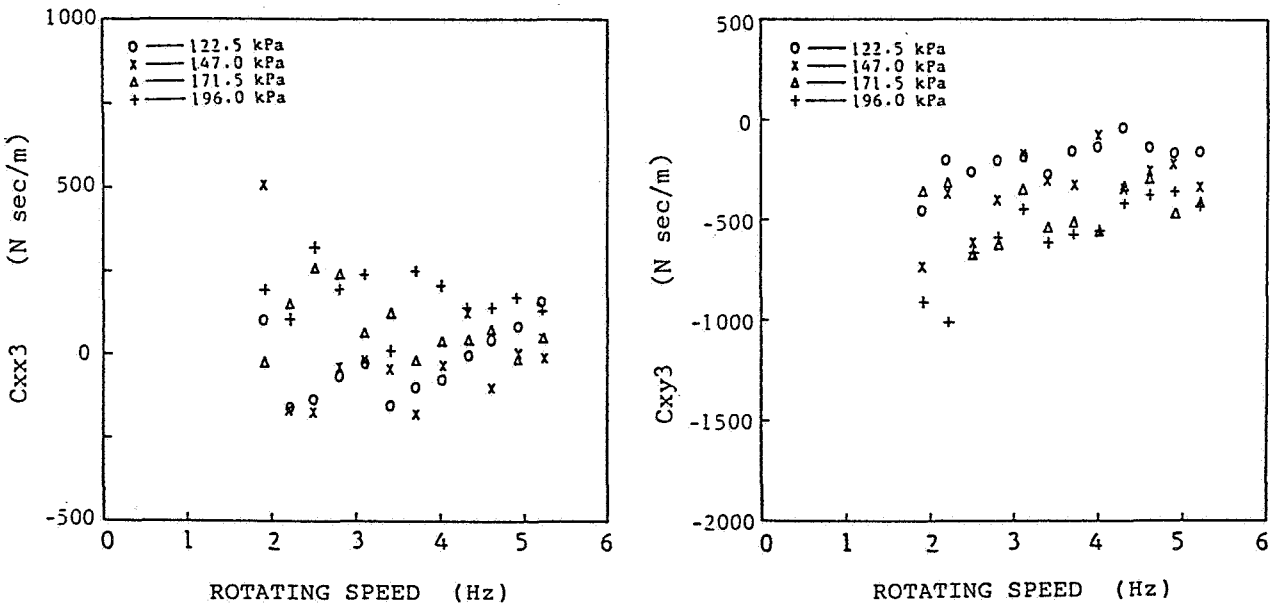

Figure 25. - Damping coefficients in the 3rd chamber

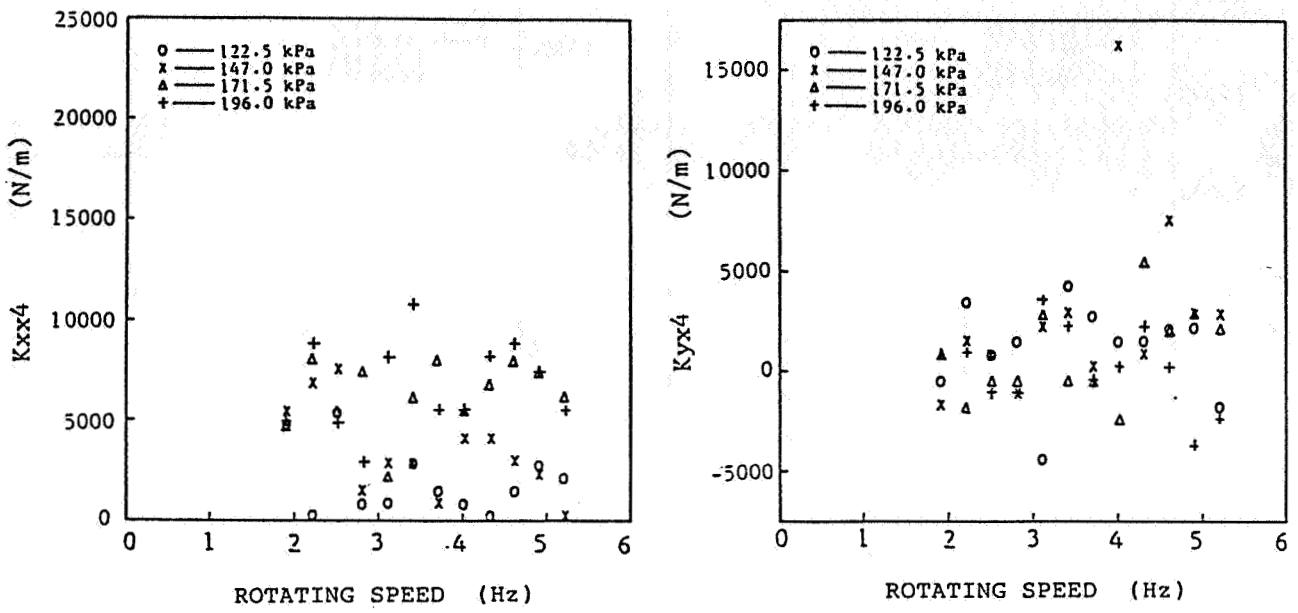

Figure 26.- Spring coefficients in the 4th chamber

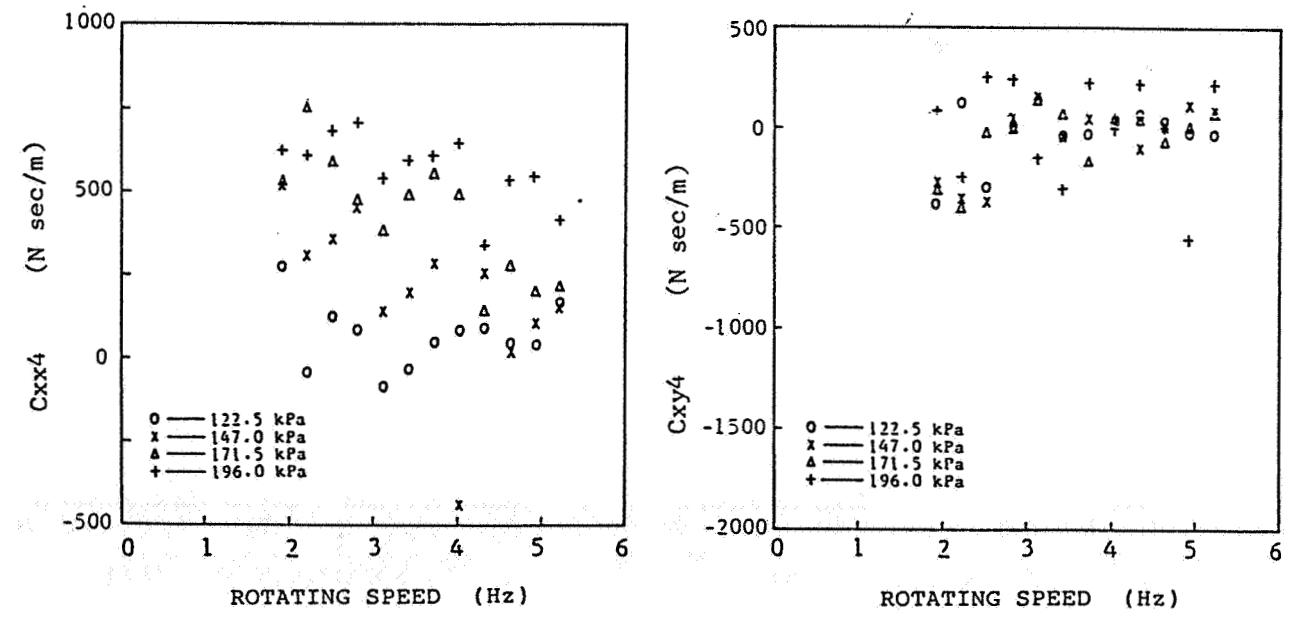

Figure 27. - Damping coefficients in the 4th chamber

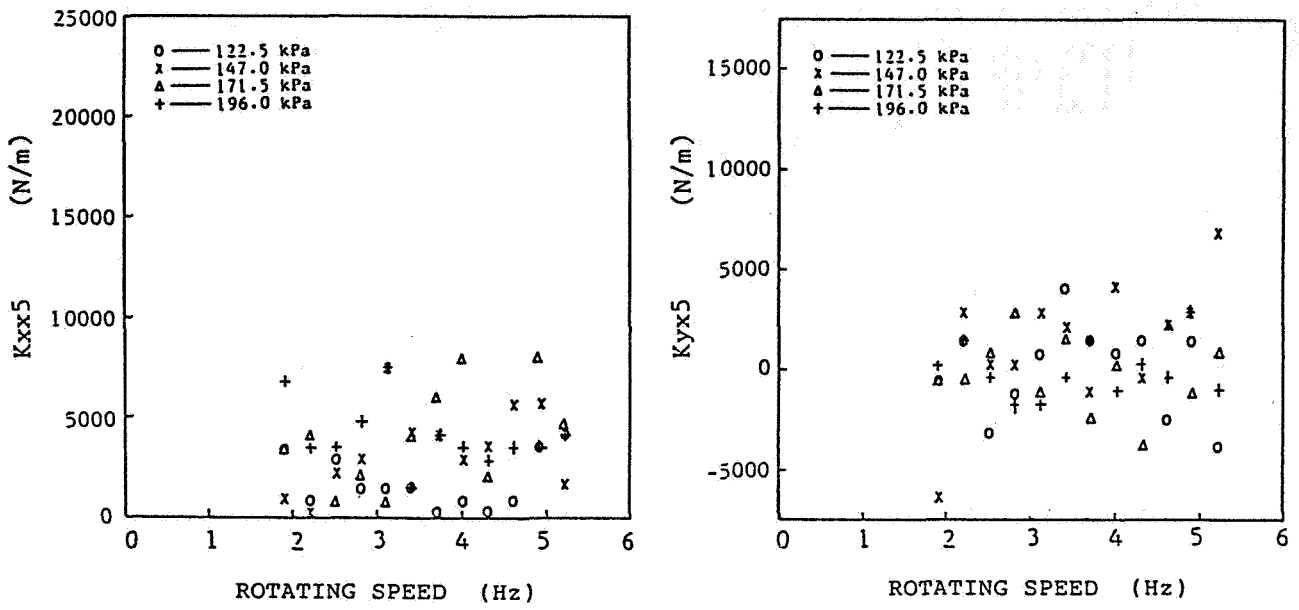

Figure 28. - Spring coefficients in the 5th chamber

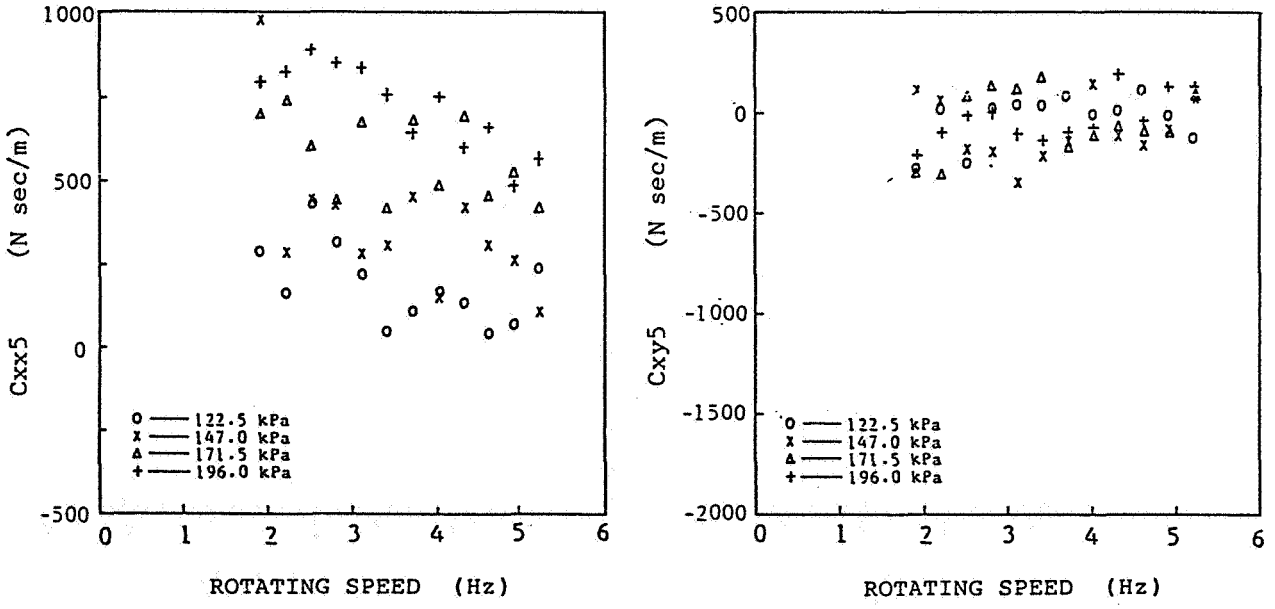

Figure 29. - Damping coefficients in the 5th chamber

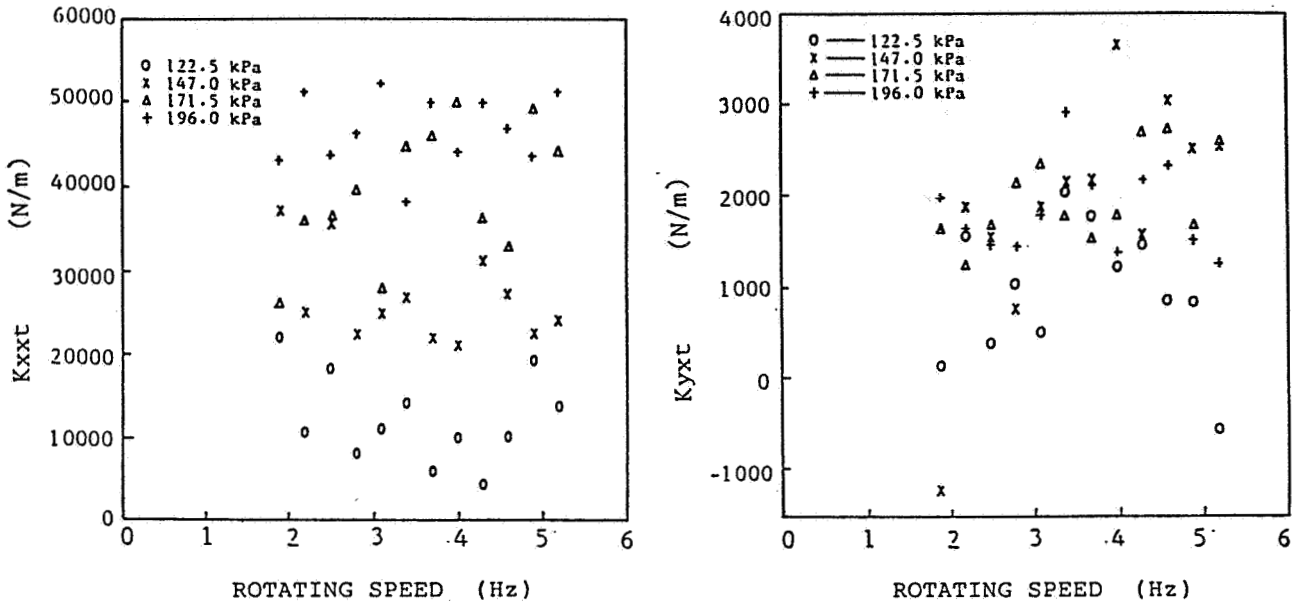

Figure 30. - Spring coefficients in the whole labyrinth seal.

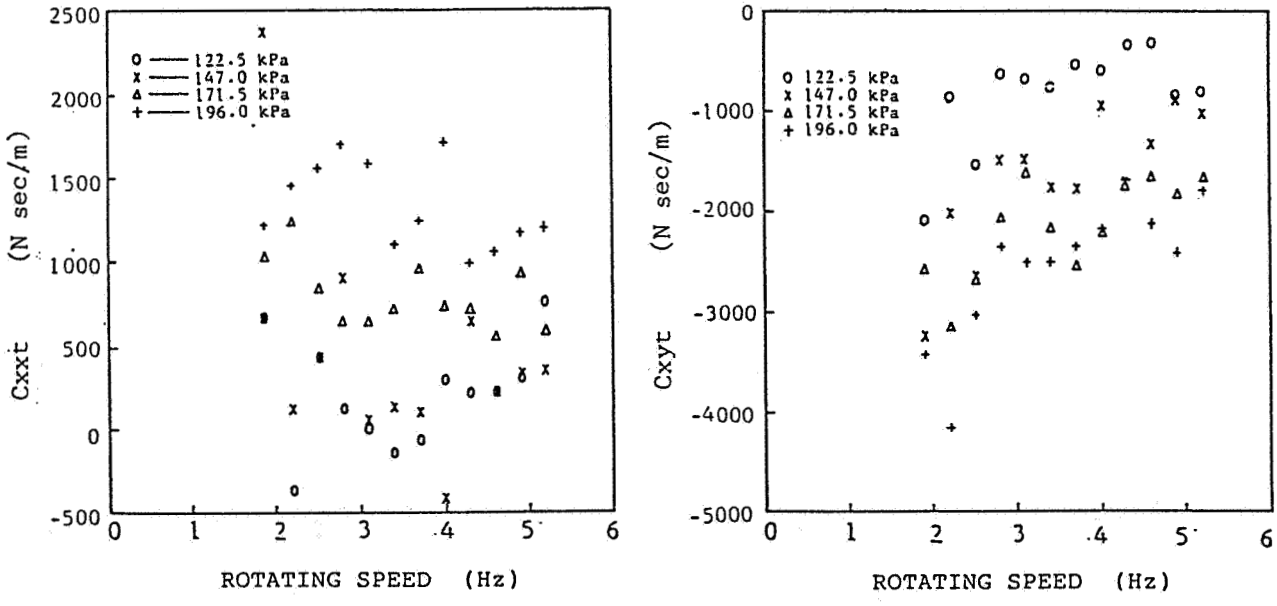

Figure 31. - Damping coefficients in the whole labyrinth seal.